Sigma Journal of Engineering and Natural Sciences
Web page info: https://sigma.yildiz.edu.tr
DOI: 10.14744/sigma.2026.2069

Research Article

Two level stochastic planning approach for renewable energy sources and capacitors allocation in distribution network considering network reconfiguration

Abhilasha PAWAR[1,*], Rajkumar VIRAL[1], Divya ASIJA[1], Mohit BANSAL[2]

[1]*Department of Electrical and Electronics Engineering, Amity School of Engineering and Technology, Amity University, Noida, Uttar Pradesh, 201313, India*
[2]*Department of Electrical and Electronics Engineering, G.L. Bajaj Institute of Technology and Management, Greater Noida, Uttar Pradesh, 201306, India*

ARTICLE INFO

Article history
Received: 12 July 2024
Revised: 21 August 2024
Accepted: 06 March 2025

Keywords:
Capacitor Banks; Power Loss Minimization; Renewable Energy Sources; Solar Photovoltaic

ABSTRACT

This research presents a novel two-level coordinated optimization model for the integrated operation and planning of capacitors and renewable energy sources (RES), specifically wind and solar photovoltaic (PV)-based distributed generation (DG), while incorporating network reconfiguration (NR). The first level optimizes the allocation of RES and capacitor devices, whereas the second level manages the scheduling of active and reactive power for RES and capacitors, along with NR operation. The proposed methodology is designed to reduce investment and operational expenditures encompassing costs associated with electricity procurement from substations, carbon emissions, unserved energy, and power losses. To address uncertainties in load demand and RES generation, a stochastic module is implemented. The framework has been tested on both the IEEE 33-bus and IEEE 69-bus distribution systems under various scenarios and solved using the proposed multi-layer Crayfish Optimization Algorithm (COA). The results reveal that the proposed framework operates effectively, with costs going down by about 50% in IEEE 33-bus system and a 60% in the IEEE 69-bus system. Also, a comparison with existing methods in the literature shows the superiority of the proposed method, with a 96.09% loss reduction compared to the base case. These improvements make the network more efficient, reliable, and flexible while significantly cut down the carbon emissions.

Cite this article as: Pawar A, Viral R, Asija D, Bansal M. Two level stochastic planning approach for renewable energy sources and capacitors allocation in distribution network considering network reconfiguration. Sigma J Eng Nat Sci 2026;44(3):1868−1887.

INTRODUCTION

Renewable energy sources (RESs) are essential for achieving environmental sustainability and will play a significant part in future distribution systems [1,2]. Though, their large-scale amalgamation poses technical challenges related to stability, reliability, and power quality.

***Corresponding author.**
*E-mail address: abhilasha.pawar@gmail.com

This paper was recommended for publication in revised form by Editor-in-Chief Ahmet Selim Dalkilic

Published by Yıldız Technical University Press, İstanbul, Turkey

The variability and uncertainty introduced by RESs complicate the operation, and planning of distribution networks and affect allocation of capacitor banks (CBs) [3]. Arbitrary placement of RES and CB units can lead to increased power flow on feeders, causing network congestion and higher losses. Planning for the expansion of distribution with RES and CB units can change the system voltage profile a lot. This can cause problems like overvoltage, undervoltage, higher system losses, and too much wear on CBs [4]. So, to get the most out of the system, it is important to carefully plan how to allocate RES and CB with network reconfiguration (NR) [5,6]. The extensive use of RESs can cause severe difficulties with voltage profiles because of reverse power flow. Their intermittent characteristics and unpredictable load behavior possibly will also induce voltage variations [7]. In [8], the techno-economic as well as environmental concern of the Karabuk University microgrid was simulated and evaluated using HOMER (Hybrid Optimization Models for Energy Resources) software. The study focused on optimization, sensitivity analysis, demand response, and pollutant emissions. Also, [9] problems in microgrids and to fix these problems with controlling reactive power from RESs and CBs work along with the NR.

In literature study, various optimization methodologies [1-25] for the efficient allocation of distributed generations (DGs) within distribution systems to reduce power losses. An improved particle swarm optimization (IPSO) technique was suggested in [1] for power loss minimization. Mountain gazelle optimization algorithm (MGOA) was used in [2] for minimizing voltage deviation, active power losses, and greenhouse gas emissions, as well as reducing electricity purchase costs. In [3] modified grey wolf optimization has been suggested for multiple capacitor allocation for system cost minimization. Similarly, the dingo optimization algorithm (DOA) was adopted in [5] for enhancing the execution of the distribution system via photovoltaic DG allocation. In [6], metaheuristic techniques such as particle swarm optimisation (PSO) and genetic algorithm (GA) were used to minimise annual energy losses and voltage variation. In [10], two hybrid approach has been introduced for multiple allocation of distributed generators for loss reduction. A Multi-objective Bidirectional Co-evolutionary algorithm (BiCo) was proposed in [11] for multiperiod DG allocation and reconfiguration to reduce various costs. The combination of Marine Predators Algorithm (MPA) and voltage stability index (VSI) was utilized in [12] for the combined allocation of DGs, capacitor banks, and electric vehicles. Geometric Mean Optimization (GMO) was adopted with the loss sensitivity index in [13] to reduce active power loss and voltage variations during network reconfiguration and the allocation of distributed generation (DG) units.

Reference [14] employed the Andean Condor Algorithm (ACA) to obtain the best place for DG and NR to decrease on power losses. In [15], the Honey Badger Algorithm (HBA) was adopted to allocate renewable DGs along with network reconfiguration to lower greenhouse gas emissions and power losses. The Wild Horse Optimizer (WHO) was employed in [16] to syndicate DGs and capacitor banks with NR in order to lower the voltage deviation as well as active power loss reduction. The Success History Based Adaptive Differential Evolution Algorithm (SHADE) was used in [17] to improve DG hosting capacity. In [18], the Grasshopper Optimization Algorithm (GOA) was employed to obtain the efficient way to use hybrid renewable energy resources. Finally, [19] employed information gap decision theory (IGDT) to include uncertainty in renewable energy and loads. The improved salp swarm algorithm (SSA) was adopted to obtain the optimal allocate PV and wind-based DGs. In [20], Binary Particle Swarm Optimization (BPSO) was employed to challenge the issue of power loss in distribution systems through the optimization of the placement and sizing of Distributed Generation (DG) units and shunt capacitor (SCs), incorporation of network reconfiguration. In the same way, the LSHADE-EpSin algorithm was used in [21] to improve network reconfiguration along with the placement of DGs and SCs.

In [22], a methodology was shown that used the Andean Condor Algorithm (ACA) and Network Reconfiguration (NR) to obtain optimal locations for DGs. In [23], the Gazelle Optimization Algorithm (GOA) and Mountain Gazelle Optimization Algorithm (MGOA) were used to obtain optimal location of DGs and capacitors in distribution networks. The Electric Eel Foraging Optimization (EEFO) algorithm was used in [24] for optimal reconfiguration as well as distributed generation (DG) placement in radial distribution networks across various practical load models. The Crayfish Optimization Algorithm was employed in [25] to obtain the optimal network configuration setup as well as optimal allocation of compensating devices such as DGs and SCs. The main goal was to improve system performance by lowering power losses and improving voltage profiles.

However, prior research [1-25] has inadequately addressed the economic, operational, and environmental factors, nor have they tackled the uncertainties in load demand and solar irradiance through a stochastic model. The combined allocation of renewable energy sources (RES) with non-renewable resources (NR) has not been thoroughly investigated from both technical and non-technical perspectives. Moreover, the impact of practical voltage-dependent load models on the allocation of RES and NR has not yet been explored. The problem formulated in this paper represents both the planning and operation of RES and NR, which constitutes a large-scale mixed-integer nonlinear programming problem. While the authors in [1-25] have employed single-stage optimization solvers, these solvers often lead to local optima due to the complexity of integrating both the planning and operational stages. This paper aims to address these gaps.

- Developed a two-level stochastic planning approach for the best allocation of renewable energy sources and capacitors.
- Implemented a comprehensive planning model for RES and CBs that takes into consideration operational, economic, and environmental factors. This model completely incorporates the uncertainties of load, wind speed and solar irradiance through a stochastic module.
- Analyzed the influence of integrated Network Reconfiguration (NR) schemes and practical load models on the allocation of RES and CBs.
- Introduced a multi-layer crayfish optimisation algorithm (COA) as a solution for solving complex non-convex mixed integer nonlinear programming (MINLP) problems, eliminating the need for linearization or relaxation techniques.
- Verified the suggested technique by applying it to the widely recognised IEEE 33-bus and IEEE 69 bus distribution systems.

MODELLING UNCERTAINTIES OF RES AND LOAD

Photovoltaic (PV) Power Generation Uncertainty

The fluctuation of solar irradiance has been represented in this study using the Beta distribution function [26], and Equation (1) gives the probability density function (PDF).

$$PDF_s(\xi) = \begin{cases} \frac{\Gamma(\alpha+\beta)}{\Gamma(\alpha)\Gamma(\beta)}\xi^{(\alpha-1)}(1-\xi)^{(\beta-1)}; 0 \le \xi \le 1, \alpha, \beta \ge 0 \\ 0 \qquad\qquad otherwise \end{cases} \tag{1}$$

Here, Γ() represents the gamma function, ξ denotes solar irradiance, β and α are parameters. These parameters are derived from (σ) standard deviation and the (μ) mean of the ξ is given in (2)

$$\beta = (1-\mu)\left(\frac{\mu(1+\mu)}{\sigma^2} - 1\right)\ ; \quad \alpha = \frac{\mu\times\beta}{1-\mu} \tag{2}$$

Each photovoltaic module›s power output is contingent upon solar irradiation, ambient temperature, and the module›s physical attributes. Equation (3) presents a power characteristic model that can be used to compute the output power.

$$P_{pv} = P_{std}\left\{\frac{\xi}{1000}[1 + \delta(T_{cell} - 25)]\right\} \tag{3}$$

$$T_{cell} = T_{amb} + \left(\frac{OCT^{nom}-20}{800}\right)\xi \tag{4}$$

Wind Power Generation Uncertainty

The weibull distribution has been utilized to represent the variability of wind speed [26], with the PDF provided in equation (5)

$$PDF_w(V) = \left(\frac{k}{c}\right)\left(\frac{v}{c}\right)^{(k-1)} exp\left(-\left(\frac{v}{c}\right)^k\right) \tag{5}$$

Here, k and c are the parameters of the Weibull distribution, and v represents speed of wind.

Equations (6) and (7) are used to determine the wind turbine›s (WT) output power.

$$P_{WG} = \begin{cases} 0; & 0 \le v < v_{ci} \\ a + b\times v^3; & v_{ci} \le v < v_{rated} \\ P^n_{WG,rated}; & v_{rated} \le v < v_{co} \\ 0; & v_{co} \le v \end{cases} \tag{6}$$

$$\left.\begin{aligned} a &= \frac{(P^n_{WG,rated}\times v^3_{ci})}{(v^3_{ci} - v^3_{rated})} \\ b &= \frac{P^n_{WG,rated}}{(v^3_{rated} - v^3_{ci})} \end{aligned}\right\} \tag{7}$$

Exponential Load Modelling

Load-to-voltage sensitivities are represented using the exponential load model (ELM) [27]. Equation (8) and (9) are employed to exhibit the active and reactive power loads.

$$P_L = P_L^{act}\left(\frac{V}{V^{act}}\right)^{k^p} \tag{8}$$

$$Q_L = Q_L^{act}\left(\frac{V}{V^{act}}\right)^{k^q} \tag{9}$$

Equations (10) and (11), which specify the active load (P_L) and reactive power loads (Q_L), respectively, are used to express the uncertainty of loads using the Normal probability distribution function (PDF) [24].

$$PDF_{pl}(P_L) = \frac{1}{\sqrt{2\pi}\sigma_p} exp\left[-\frac{(P_L^{act} - \mu_p)^2}{2\sigma_p^2}\right] \tag{10}$$

$$PDF_{ql}(Q_L) = \frac{1}{\sqrt{2\pi}\sigma_q} exp\left[-\frac{(Q_L^{act} - \mu_q)^2}{2\sigma_q^2}\right] \tag{11}$$

Stochastic Variable Module for Uncertainties Modelling

To represent the uncertainty of variables like solar irradiance, wind speed and load, the stochastic variable module [28] was introduced. The probability distribution (PDF) of each random variable (i.e. load, wind speed and solar irradiance, is divided into several intervals as shown in Figure 1(a), each of which is associated with a standard deviation (σ) and a probability ($\alpha^L_{l,s}$, $\alpha^{Wd}_{l,s}$ and $\alpha^{PV}_{l,s}$). A roulette wheel, as shown in Figure 1(b), has been used to model each probability level with a particular stochastic variable. Using this process, a random number between 0 and 1 is produced. The interval on the roulette wheel is determined by this random number, which also indicates the forecast error and the likelihood that it has with respect to the random variable (wind speed, load, and sun irradiance, for example). To produce the necessary number of scenarios, the same process is repeated (Ns). The properties of the PV module are then used to translate solar irradiance into PV power generation, while the characteristics of the wind turbine are used to convert wind speed into wind power generation. Equations (12) and (13) reveal the arrangement of the s^{th} scenario and the related normalised probability.

$$s = \left[P^{Wd}_{i,s}, P^{L}_{j,s}, P^{PV}_{k,s}\right]; \forall\{i\epsilon\Omega_W, j\epsilon\Omega_{bus}, k\epsilon\Omega_{PV} \tag{12}$$

$$Pr\,o\,b(s) = \frac{\left(\Pi_{L=1}^{N_L}(\alpha^{L}_{l,s})\right)\left(\Pi_{PV=1}^{N_{PV}}(\alpha^{PV}_{l,s})\right)\left(\Pi_{Wd=1}^{N_{Wd}}(\alpha^{Wd}_{l,s})\right)}{\sum_{s=1}^{N_s}\left(\left(\Pi_{L=1}^{N_L}(\alpha^{L}_{l,s})\right)\left(\Pi_{PV=1}^{N_{PV}}(\alpha^{PV}_{l,s})\right)\left(\Pi_{Wd=1}^{N_{Wd}}(\alpha^{Wd}_{l,s})\right)\right)} \tag{13}$$

It is crucial to acknowledge that as the quantity of situations grows, the amount of time required for computing also increases. An effective scenario reduction method is necessary for the distribution system operator (DSO) to quickly find control variable values that align with the hourly operational schedule, to reduce calculation time. In order to tackle this issue, the K-means clustering technique has been devoted to decrease the quantity of situations. The objective of this algorithm is to categorise novel situations of uncertainties by their commonalities. Each cluster›s centroid represents the average value of uncertainties within that cluster. After applying this scenario reduction technique, the probability of the resultant decreased scenarios (N_{ds}) is standardised by Equation (14).

$$\pi_s = \frac{Pr\,ob(s)}{\sum_{s=1}^{N_{ds}} Pr\,ob(s)}; \forall s = 1,2,\ldots N_{ds} \tag{14}$$

Objective Function

The suggested methodology aims to minimise the total cost, which can be represented as Equation (15).

$$min.\,O\,F = \overbrace{IC}^{I} + \overbrace{OC + EPC + EM + EL + ENS}^{II} \tag{15}$$

In Equation (15), part I represents the investment cost (IC) of capacitors, wind turbines, and photovoltaic (PV) based distributed generation units, which are determined in level 1 (integrated planning level). However, part II indicates the overall predicted variable costs, which under all potential operational scenarios comprise the energy not served (ENS), energy purchase costs (EPC), emission costs (EC), energy loss (EL) cost, and operating expenses (OC) of these units.

The calculated expression for the investment cost (IC) is as follows:

$$IC = \begin{bmatrix} AC^{Cap}\sum_{i\in\Omega_{cap}}\left(C^{inv}_{cap}Q^{rated}_{cap,i}\right) \\ +AC^{Wd}\sum_{ij\in\Omega_{Wd}}\left(C^{inv}_{Wd}P^{rated}_{Wd,i}\right) \\ +AC^{PV}\sum_{ij\in\Omega_{PV}}\left(C^{inv}_{PV}P^{rated}_{PV,i}\right) \end{bmatrix} \tag{16}$$

Where, $AC^x = \frac{d(1+d)^{LTx}}{(1+d)^{LTx-1}}; x \in \{cap, wind, PV\}$

AC signifies the annual cost. Here, *d* represents the rate of discount and *LT* signifies the asset's lifetime period. In Equation (16), the first line denotes the cost of capacitors,

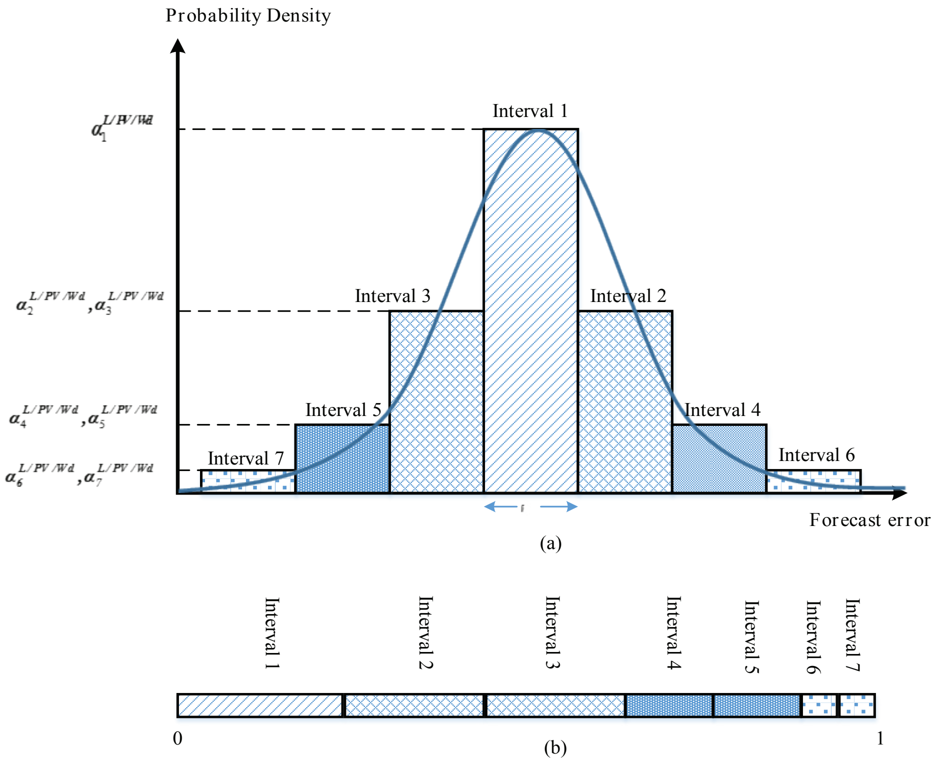

Figure 1. (a) Standard division of the PDF for PV/load/wind forecast errors (b) Mechanism of roulette wheel.

while the second and third lines signifies the annual cost of wind and PV based DG units, respectively.

The following mathematical formulas can be used to determine level 2 since it entails incorporated operation optimisation via repeated simulations to minimise the predicted variable expenses, which are given in (17).

$$OC = \left[\sum_{t=1}^{T}\left(\sum_{s=1}^{N_{ds}}\pi_s \times \begin{pmatrix}\sum_{i\in\Omega_{cap}} C_{cap}^{OM,t} Q_{cap,i,s}^{t} + \sum_{i\in\Omega_{Wd}} C_{Wd}^{OM,t} P_{Wd,i,s}^{t} \\ + \sum_{i\in\Omega_{PV}} C_{PV}^{OM,t} P_{PV,i,s}^{t}\end{pmatrix}\right)\right] \times D_y \quad (17)$$

$$EPC = \left[\sum_{t=1}^{T}\left(\sum_{s=1}^{N_{ds}}\pi_s \times \left(C_{sub}^{t} P_{sub,s}^{t}\right)\right)\right] \times D_y \quad (18)$$

$$EC = \left[\sum_{t=1}^{T}\left(\sum_{s=1}^{N_{ds}}\pi_s \times \left(C_{emis} P_{sub,s}^{t}\right)\right)\right] \times D_y \quad (19)$$

$$EL = \left[\sum_{t=1}^{T}\left(\sum_{s=1}^{N_{ds}}\pi_s \times \left(C_{loss} P_{loss,s}^{t}\right)\right)\right] \times D_y \quad (20)$$

$$ENS = \left[\sum_{t=1}^{T}\left(\sum_{s=1}^{N_{ds}}\pi_s \times \left(C_{ens} P_{ens,i,s}^{t}\right)\right)\right] \times D_y \quad (21)$$

Constraints

The following requirements for the operational and planning models must be met.

- Limit installation of capacitors, wind turbines, and photovoltaic (PV) based distributed generation units at each bus

$$\left.\begin{array}{l} 0 \le Q_{cap,i}^{rated} \le Q_{cap,i}^{max} \\ 0 \le P_{Wd,i}^{rated} \le P_{Wd,i}^{max} \\ 0 \le P_{PV,i}^{rated} \le P_{PV,i}^{max} \end{array}\right\} \quad (22)$$

- constraints of power flow

$$\left.\begin{array}{l} P_{i,s}^{t} = V_{i,s}^{t}\sum_{i\in\Omega_{bus}} V_{j,s}^{t}\left(G_{ij}\cos\theta_{ij,s}^{t} + B_{ij}\sin\theta_{ij,s}^{t}\right) \\ Q_{i,s}^{t} = V_{i,s}^{t}\sum_{i\in\Omega_{bus}} V_{j,s}^{t}\left(G_{ij}\sin\theta_{ij,s}^{t} - B_{ij}\cos\theta_{ij,s}^{t}\right) \end{array}\right\} \quad (23)$$

Where

- constraints of voltage for each scenario

$$V^{min} \le V_{i,s}^{t} \le V^{max} \quad (24)$$

- constraints of branch capacity

$$0 \le I_{l,s}^{t} \le I_{l}^{rated} \quad (25)$$

- Load Modelling:

$$P_{i,s}^{D,t} = P_{act,i,s}^{D,t}\left(\frac{V_{i,s}^{t}}{V_{act,i,s}}\right)^{k^p} \quad (26)$$

$$Q_{i,s}^{D,t} = Q_{act,i,s}^{D,t}\left(\frac{V_{i,s}^{t}}{V_{act,i,s}}\right)^{k^q} \quad (27)$$

Overview Of Crayfish Optimization Algorithm

Crayfish Optimization Algorithm (COA) [29] is inspired by the foraging, vacationing, and competitive behaviors of crayfish. The algorithm mimics the crayfish›s ability to handle food using their claws and walking feet, as well as their defensive mechanisms. The COA›s exploitation phase is represented by the foraging and competition stages, and its exploration phase is represented by the summer vacation period. The positions of each crayfish indicate a possible solution, and the algorithm defines a colony of crayfish. The temperature of the surrounding air regulates the change from the exploration to the exploitation phase. The ideal food position is represented by the optimal solution during foraging, which is determined by simulating the crayfish›s alternating eating behaviours using sine and cosine formulas. The five steps of the COA are as follows:

Stage 1: Initialization

The first stage of the COA entails randomly generating a located of candidate keys, referred to as *Cf*, within the defined search space. These candidate solutions, *Cf*, are created based on the population size (N) and dimensionality (*dim*). The initialization of the COA can be described in Equation (28).

$$Cf = \begin{bmatrix} Cf_{1,1} & \cdots & Cf_{1,dim} \\ \vdots & \ddots & \vdots \\ Cf_{N,1} & \cdots & Cf_{N,dim} \end{bmatrix} \quad (28)$$

Here, C_f represents the initial positions of the population. The position of the i-th individual in the j-th dimension is denoted by $Cf_{i,j}$, and it is computed using Equation (29)

$$Cf_{i,j} = lb_{i,j} + (ub_{i,j} + lb_{i,j}) \times rand \quad (29)$$

Here, lb_{ij} and ub_{ij} represent lower and upper limits of the j-th dimension, while *rand* denotes a random number.

In this case, *rand* stands for a random integer, and , lb_{ij} and ub_{ij} indicate the lower and upper limits of the j-th dimension.

Stage 2: Impact of temperature on crayfish consumption

Crayfish undergo distinct stages of behaviour due to variations in temperature. In Equation (30), the temperature is defined. Crayfish seek cooler spots for the summer as the temperature rises above 30°C. When the temperature is ideal, crayfish will forage, and the temperature will affect how much they eat. Crayfish prefer to feed in the range of 15°C to 30°C, with 25°C being the best temperature. As a result, feeding quantity is temperature-dependent and roughly follows a normal distribution since crayfish exhibit robust foraging behaviour between 20°C and 30°C. As a result, the temperature range specified by the COA is 20°C to 35°C. Equation (31) is the mathematical model for crayfish intake.

$$Temp = rand \times 15 + 20 \quad (30)$$

$$p = W \times \left(\frac{1}{\sqrt{2\times\pi}\times\sigma} \times exp\left(-\frac{(Temp-\mu)^2}{\sigma^2}\right)\right) \quad (31)$$

Here, μ represents the optimal crayfish temperature, while σ and W are used to adjust the extent of crayfish utilized at various temperatures.

Stage 3: Exploration

The crayfish cannot withstand temperatures higher than 30°C. They decide at this moment to stay in the cave for the summer. The cave, (Cf_{shade}), is given in (32)

$$Cf_{shade} = \frac{Cf_G + Cf_L}{2} \quad (32)$$

In this case, (Cf_L) indicates the ideal position within the current population, while (Cf_G) indicates the best position attained by cumulative iterations.

The phenomenon of crayfish waging territorial wars inside caves is seen as random. The crayfish can enter the cave straight for the summer if there are no competing crayfish, as indicated by a random variable (*rand*) value less than 0.5. This process is modelled in (33)

$$Cf_{i,j}^{it+1} = Cf_{i,j}^{it} + S \times (Cf_{shade} - Cf_{i,j}^{it}) \quad (33)$$

it represents the current iteration. Furthermore, *S* is a declining curve, as illustrated in (34)

$$S = 2 - \left(\frac{it}{IT_{max}}\right) \quad (34)$$

Here, IT_{max} represents the maximum number of iterations.

Stage 4: Exploitation

If the temperature rises beyond 30 degrees and the *rand* value is below 0.5, it suggests that the cave is attracting organisms other than crayfish. Equation (35) depicts the crayfish engaging in competition to gain dominance over the cave.

$$Cf_{i,j}^{it+1} = Cf_{i,j}^{it} - Cf_{z,j}^{it} + Cf_{shade} \quad (35)$$

Here, Cf_{ij} represents a randomly chosen crayfish individually

$$z = round\big(rand \times (N-1)\big) + 1 \quad (36)$$

Crayfish compete among themselves, and each crayfish Cf_i adjusts its position based on the location of additional crayfish (Cf_z). This change in position widens the COA›s hunt scope, thus improving the algorithm›s ability to explore.

Stage 5: Phase of foraging

Feeding of crayfish is deemed suitable when temperatures are at or below 30°C. During this stage, crayfish display robust movement as they approach the food source. Upon encountering the food, crayfish assess the size of the food item. They employ their claws to disassemble large food pieces and then consume them by alternating between their second and third walking limbs.

$$Cf_{food} = Cf_G \quad (37)$$

The dimension of food Q is represented as:

$$Q = k \times rand \times \left(\frac{fitness_i}{fitness_{food}}\right) \quad (38)$$

Here, k stands for the food factor, indicating the limit size of food with a fixed value of 3. $fitness_i$ correspond to the fitness value of the i-th crayfish, and $fitness_{food}$ is the fitness value linked to the food›s location.

The crayfish assesses food size centered on the significant food item›s dimensions. If $Q > (k+1)/2$, it suggests that the food section size is excessive. Currently, the crayfish is tearing its food employing its primary claw addition. This process is simulated by the following Equation

$$Cf_{food} = exp\left(-\frac{1}{Q}\right) \times Cf_{food} \quad (39)$$

The equation describing foraging, with the connection between food acquired by crayfish and their food intake, is given in Equation (40)

$$Cf_{i,j}^{it+1} = Cf_{i,j}^{it} + Cf_{food} \times p \times \big(cos(2\times\pi\times rand) - sin(2\times\pi\times rand)\big) \quad (40)$$

When $Q > (k+1)/2$, crayfish can directly attempt the food and use it without any additional steps. This scenario can be described by the following Equation

$$Cf_{i,j}^{it+1} = \big(Cf_{i,j}^{it} - Cf_{food}\big) \times p + p \times rand \times Cf_{i,j}^{it} \quad (41)$$

Crayfish utilize various feeding approaches established on the size of their food (Q), where the food (Cr_{food}) signifies the optimum solution. *Q* is suitable for crayfish consumption; they approach food directly. If Q, is too greater, it shows a pointed gap between the crayfish and the ideal solution. So, efforts are made to reduce the prevalence of (Cr_{food}) and bring it closer to the food item. Through the foraging phase, the COA algorithm aims to achieve the optimal key, thereby enhancing its exploitation capability and demonstrating concentrated convergence abilities. The procedure of COA is showed in Table 1.

Proposed Multi Level COA Solution Technique

The research focuses on solving a complex and difficult large-scale, MINLP problem using unconventional optimisation strategies. To tackle this, the problem is divided into two models: the planning model and the operation model. Figure 2 illustrates the multi level COA solution methodology, where Level 1 and Level 2 are governed by control sets C1 and C2, correspondingly. Set C1 includes candidate solutions for the installation of RES and capacitors. Set C2

Table 1. Algorithm 1. Pseudo-Code of COA

Step 1. Initialize variables: Maximum iterations, Population, dimension
Step 2. Generate candidate solutions utilizing equations (28) and (29).
Step 3. Calculate fitness quantities to determine Cr_G and Cr_L.
Step 4. While iteration (*it*) is less than maximum iterations (*IT*):
a. Define temperature using equation (30).
b. If temperature is greater than 30:
i. Define cave Cr_{shade} using equation (32).
ii. If rand is less than 0.5, crayfish engage in stage of summer resort in (33); otherwise, they compute for caves using equation (35).
c. Else:
i. Obtain nutrition intake P and food size Q using equation (31) and equation (38).
ii. If Q is greater than 2, crayfish shred food with equation (39), otherwise, they forage according to equations (40) and (41).
d. Update fitness values, Cr_G and Cr_L.
e. Increment *it* by 1.
Step 5. End While.

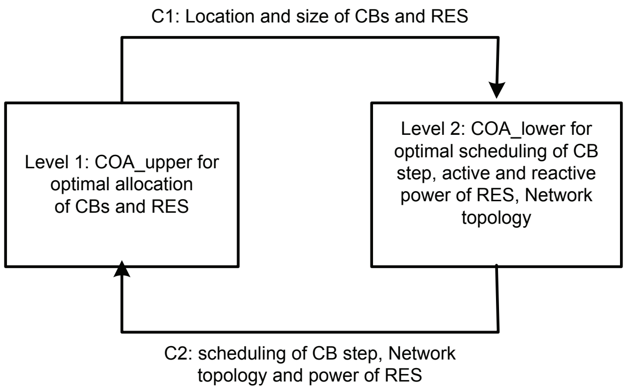

Figure 2. Multi-Level COA solution methodology.

involves the operational scheduling of RES devices, considering CB steps and remote-controlled switch statuses of network topology. Both levels are solved concurrently using the outer layer of COA optimization.

This work utilises the COA, which is an evolutionary method, to provide candidate solutions C1 within the MATLAB environment. Every candidate solution (C1) from level 1 is moved to the inner layer. At level 2, the operation sequencing of RES and capacitors is interactively solved for each hour and each potential scenario, taking into account CB steps and switch statuses, for each candidate solution C1. MINLP problem at level 2 is solved using inner COA optimisation, with the goal of minimising operational costs for the candidate installation variables offered by the COA solver in a recursive manner. The solution of level 2 provides the values of the choice variables, denoted as C2, for the scheduling of operations. These values are determined for each scenario s at hour t. The COA solver continues to iterate until it reaches convergence. Detailed pseudo code has been depicted in Table 2.

Findings and Analysis of Simulated Data

The two-level coordinated optimization model proposed in this research was implemented in the MATLAB environment. The computations were carried out on a laptop with a 2.5 GHz Core i3 processor and 4 GB of RAM.

Data

The proposed approach was evaluated using the IEEE 33-bus and 69-bus distribution networks, with load and line data sourced from [30,31]. The peak active and reactive power loads are 3715 kW, 2300 kVAR (69-bus) and 3802.19 kW, 2694.6 kVAR (33-bus), with voltage limits maintained between 0.95 pu and 1.05 pu. Figures 3 and 4 depict the respective network diagrams. In Figure 5, the typical load profile, grid power prices, and the output of wind and PV generation over 24 hours are depicted [27]. We obtained the exponential load model coefficients for different types of customers (industrial, residential, and commercial) from [32] and the wind speed and solar irradiance data from [33]. As explained in section 3, 100 scenarios were made using Monte Carlo Simulation (MCS) for scenario generation. These scenarios were then reduced to 10 using K-means clustering. Cost parameters for capacitors, wind turbines, and PV-based distributed generation units were obtained from [3] and [26]. The emission rate for bought power from the grid was set at 0.4 tCO2e/MWh, with an emission price of $60/tCO2e [22]. The distribution network was assumed to accommodate a maximum of two to three units each for installed capacitors, wind turbines, and PV-based distributed generation units.

Figure 5 depicts the typical grid power prices, load profile, and the output of PV and wind generation over 24 hours

Analysis of Numerical Data and Subsequent Conversations

The optimisation problem has been resolved successfully for five separate instances, labelled as Case 1 to Case 5, as specified in Table 3.

Table 2. Proposed multi-COA for the RES and CBs allocation problem's pseudo code

```
Input:
    Read load data, line data, and generation data of the distribution system
    Initialize parameters for both upper level (COA_upper) and lower level (COA_lower)
Initialization:
    Initiate COA_upper for optimal location and rating of RES and CBs
    Generate initial population of agents for location and size of RES and CBs within permissible limits
    Set iteration count for COA_upper
    Initiate COA_lower for scheduling of RES, CBs, and remote-controlled switches within allowable limits
    Set iteration count for COA_lower
Lower Level Optimization (COA_lower):
    While (COA_lower stopping condition is not satisfied):
        For each hour:
            Calculate fitness function by dispatching RES and CBs with network topology using equation (17)
        End For
        Evaluate COA_lower subject to constraints (6) to (11) for the current iteration
        If (COA_lower stopping condition is not satisfied):
            Perform COA_lower procedure for the current iteration
        End If
    End While
Upper-Level Optimization (COA_upper):
    Perform load flow analysis using settings obtained from COA_upper
    Evaluate fitness function by allocating RES and CBs using equation (16)
    If (COA_upper stopping criterion is not satisfied):
        Perform COA_upper procedure for the current iteration
    End If
Output:
    Location and capacity of RES and CBs
    Active and reactive power scheduling of RES and CBs
    Settings for remote-controlled switches of network topology
```

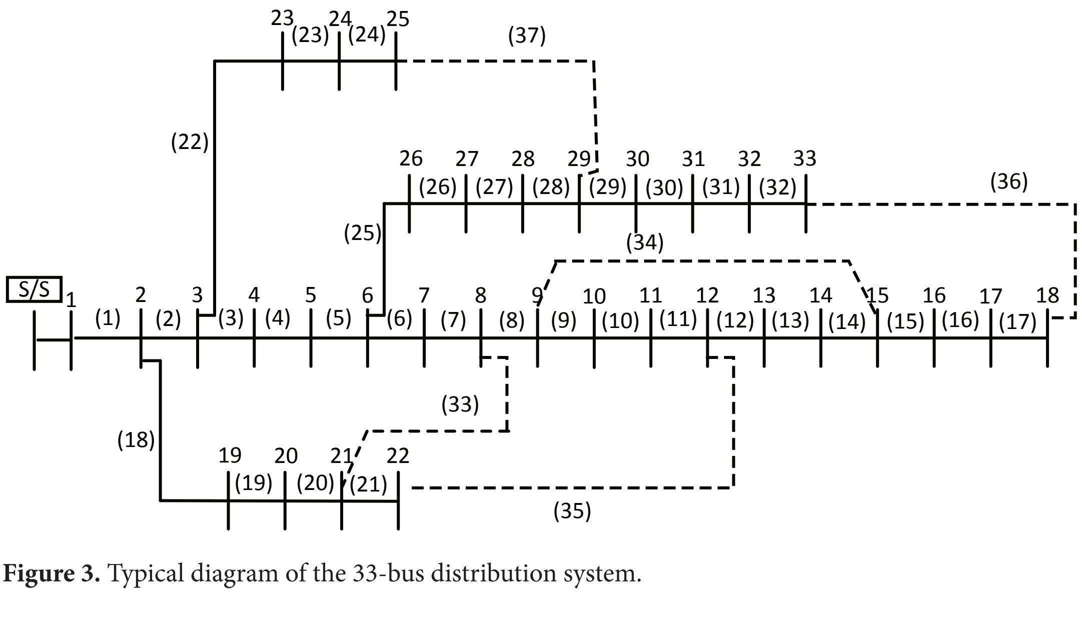

Figure 3. Typical diagram of the 33-bus distribution system.

Case 1: Base case scenario with no additional devices installed.

Case 2: Investments in capacitors.

Case 3: Investments in Renewable Energy Sources (RES), specifically PV and wind.

Case 4: Investments in RES along with capacitors.

Case 5: Investments in RES along with capacitors and network reconfiguration.

Cost Analysis Results

Tables 4 and 5 give a full picture of the IEEE 33-bus and IEEE 69-bus systems. They show that by strategically allocating resources across different investment, operational, and maintenance parameters, costs can be cut significantly.

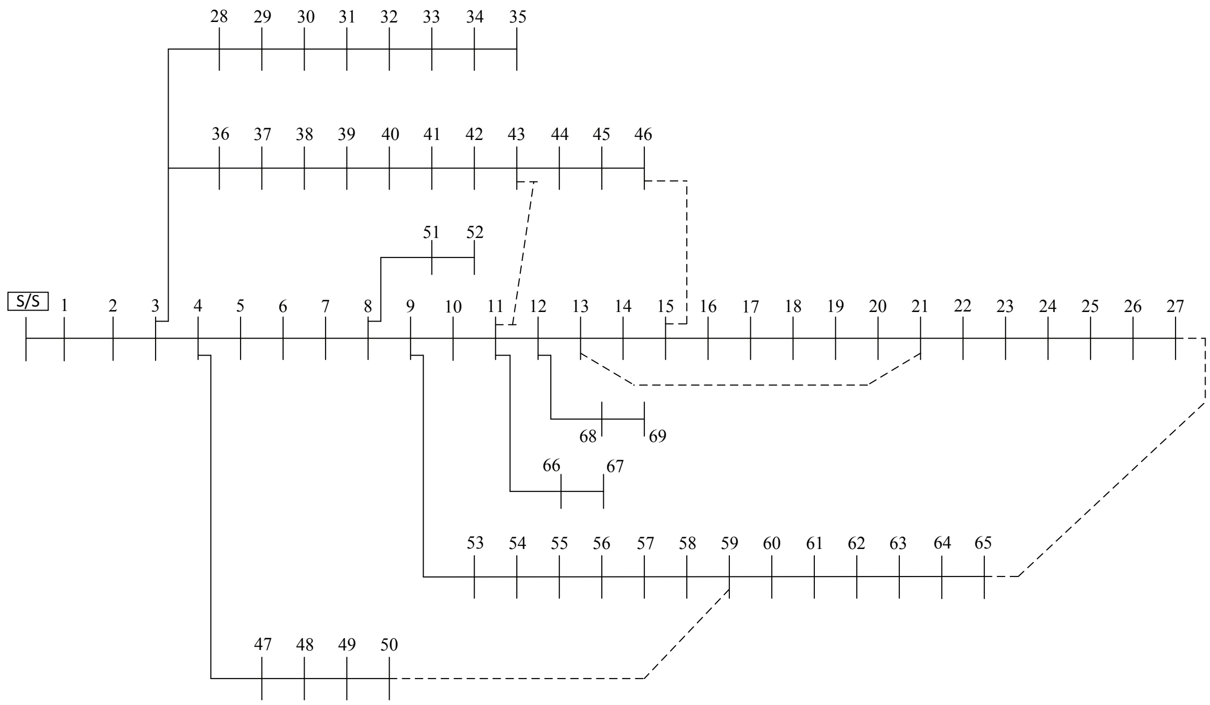

Figure 4. Typical diagram of the 69-bus distribution system.

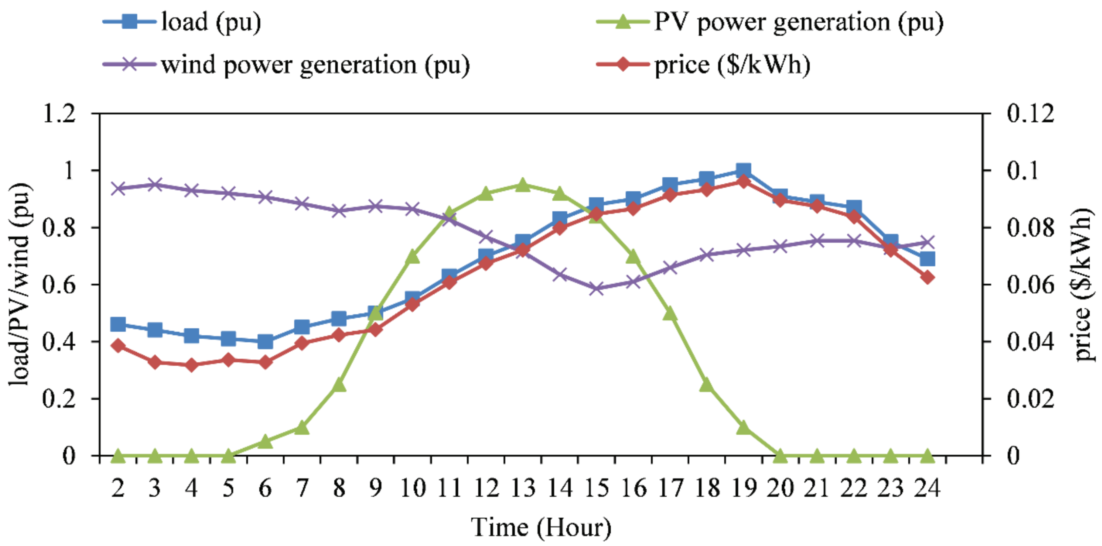

Figure 5. Sample profile of grid price, load, PV and wind generation.

The IEEE 33 bus system showed progressive cost savings: allocating capacitors saved 7.634% ($384.328), implementing RES saved 34.424% ($1,733.053), combining RES and capacitors saved 43.217% ($2,175.703), and integrating RES, capacitors, and DNR saved the most money at 50.762% ($2,555.569). The IEEE 69 bus system had even bigger benefits: capacitor allocation saved 15.699% ($934.147), RES implementation saved 43.281% ($2,575.337), combined RES and capacitors saved 58.960% ($3,508.273), and the full integration of all three parts saved the most money at 60.705% ($3,612.086). These results clearly show that integrated planning, especially when RES, capacitors, and DNR are used together, works much better than using each part on its own in both systems. The IEEE 69 bus always shows the best cost-cutting potential in all cases.

Table 3. Cases studies

CASES	CAP	RES: PV WIND	DNR
Case 1	No	No	No
Case 2	Yes	No	No
Case 3	No	Yes	No
Case 4	Yes	Yes	No
Case 5	Yes	Yes	Yes

Tables 6 and 7 give a full picture of how resources are spread out across the IEEE 33-bus and IEEE 69-bus distribution systems. They show how different case implementations lead to different patterns of capacity optimization. Case 2 starts with 1280 kVAR of capacitor banks in the IEEE 33 bus system. Case 3 uses 1100 kW of PV and 1480 kW of wind generation. In Case 4, the coordinated approach increases the capacitor capacity to 1320 kVAR while keeping the RES capacities the same (1110 kW PV, 1480 kW

Table 4. Summary of results for IEEE 33 bus distribution system

Parameters	Case 1	Case 2	Case 3	Case 4	Case 5
Investment cost ($\times10^3$ \$)	------	6.840	257.837	265.825	262.564
operational cost ($\times10^3$ \$)	------	0.900	623.360	628.142	640.757
loss cost ($\times10^3$ \$)	866.326	718.788	463.487	295.907	162.081
Energy purchased from grid ($\times10^3$ \$)	1834.289	1835.212	824.983	819.399	797.635
Reliability cost ($\times10^3$ \$)	1443.877	1197.981	772.479	493.178	270.135
Emission cost ($\times10^3$ \$)	889.912	890.356	359.206	356.251	345.663
Total cost ($\times10^3$ \$)	5034.404	4650.076	3301.352	2858.702	2478.835
Savings in total cost ($\times10^3$ \$)	------	384.328	1733.053	2175.703	2555.569
Total cost reduction (%)	------	7.634	34.424	43.217	50.762

Table 5. Summary of results for IEEE 69 bus distribution system

Parameters	Case 1	Case 2	Case 3	Case 4	Case 5
Investment cost ($\times10^3$ \$)	0.000	8.400	254.936	263.742	246.666
O & M cost ($\times10^3$ \$)	0.000	0.900	653.147	645.456	612.143
loss cost	1144.294	803.029	467.715	121.770	92.597
Energy purchased from grid ($\times10^3$ \$)	1953.074	1930.311	849.987	841.881	856.915
Reliability cost ($\times10^3$ \$)	1907.157	1338.382	779.524	202.949	154.329
Emission cost ($\times10^3$ \$)	945.737	935.094	369.618	366.192	375.528
Total cost ($\times10^3$ \$)	5950.263	5016.116	3374.927	2441.990	2338.178
Savings in total cost ($\times10^3$ \$)	------	934.147	2575.337	3508.273	3612.086
Total cost reduction (%)	------	15.699	43.281	58.960	60.705

Table 6. Location and capacity of RES and CB under different cases for IEEE 33 bus distribution system

Cases	devices	(bus#location, capacity#size (kW/kVAR))	Total size (kW/kVAR)	Opened switches for NR operation
Case 2	CB	(6,600); (11,250); (23,430)	1280	{33, 34, 35, 36,37}
Case 3	PV	(8,600); (14,500)	1100	{33, 34, 35, 36,37}
	Wind	(26,760); (32,720)	1480	
Case 4	CB	(6,600); (10,270); (23,450)	1320	{33, 34, 35, 36,37}
	PV	(16,580); (32,530)	1110	
	Wind	(22,740); (31,740)	1480	
Case 5	CB	(8,600); (15,270); (25,450)	1320	{33, 34, 10, 30, 28}
	PV	(9,570); (13,420)	990	
	Wind	(25,960); (33,610)	1570	

Table 7. Location and capacity of RES and CB under different cases for IEEE 69 bus distribution system

Cases	devices	(bus#location, capacity#size (kW/kVAR))	Total size (kW/kVAR)	Opened switches for NR operation
Case 2	CB	(11,600); (49,600); (61,600)	1800	{69, 70, 71, 72, 73}
Case 3	PV	(12,430); (62,480)	910	{69, 70, 71, 72, 73}
	Wind	(17,350); (61,1300)	1650	
Case 4	CB	(10,350); (50,560); (60,600)	1510	{69, 70, 71, 72, 73}
	PV	(16,400); (61,570)	970	
	Wind	(17,370); (62,1230)	1600	
Case 5	CB	(12,150); (51,600); (61,600)	1350	{69, 70, 14, 58, 61}
	PV	(11,450); (59,330)	780	
	Wind	(18,450); (63,1180)	1630	

wind). In Case 5, 1320 kVAR capacitors are used to show how to best use resources. The wind capacity goes up to 1570 kW, and the PV capacity goes down to 990 kW. There are also changes to the network (switches 33, 34, 10, 30, and 28). Because it is bigger, the IEEE 69 bus system needs more capacity. Case 2 has 1800 kVAR of capacitors, Case 3 has 910 kW of PV and 1650 kW of wind, and Case 4 has 1510 kVAR of capacitors with 970 kW of PV and 1600 kW of wind. The best setup for Case 5 is with 1350 kVAR capacitors, 780 kW of PV, and 1630 kW of wind. It also has smart network reconfiguration (switches 69,70,14,58,61). This shows that coordinated RES allocation with network reconfiguration could support to meet the total capacity needs without adding new resources.

Technical Analysis Results

Figures 6 and 7 illustrate the temporal analysis of power losses across the IEEE 33-bus and IEEE 69-bus systems, demonstrating significant performance improvements through progressive system enhancements.

In the IEEE 33 bus system, Case 1 (base case) exhibits peak losses of approximately 160 kW during hour 20, which reduces to about 130 kW with capacitor bank installation (Case 2), further decreasing to around 100 kW with RES integration (Case 3), achieving about 65 kW through RES and CB coordination (Case 4), and finally reaching optimal performance with peak losses around 40 kW through comprehensive optimization (Case 5).

The IEEE 69 bus system also has bigger initial losses, with Case 1 peaking at 220 kW and then going down to about 160 kW with capacitors (Case 2), 100 kW with RES (Case 3), 35 kW with combined RES and CBs (Case 4), and very small losses of ~15 kW through the integrated approach (Case 5). Both systems show the same daily patterns, with lower losses during off-peak hours (1-8 and 22-24), a gradual rise in losses during morning hours (9-12), the highest

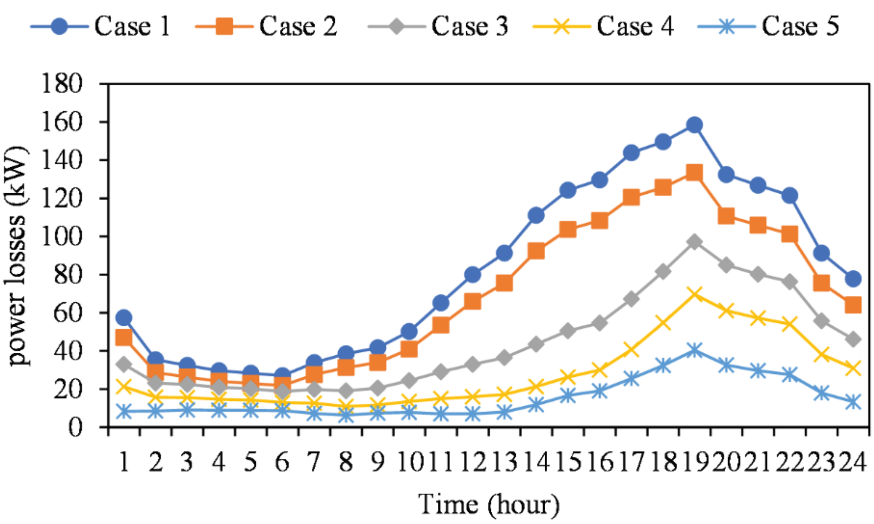

Figure 6. Active power losses across different cases For 33 bus system.

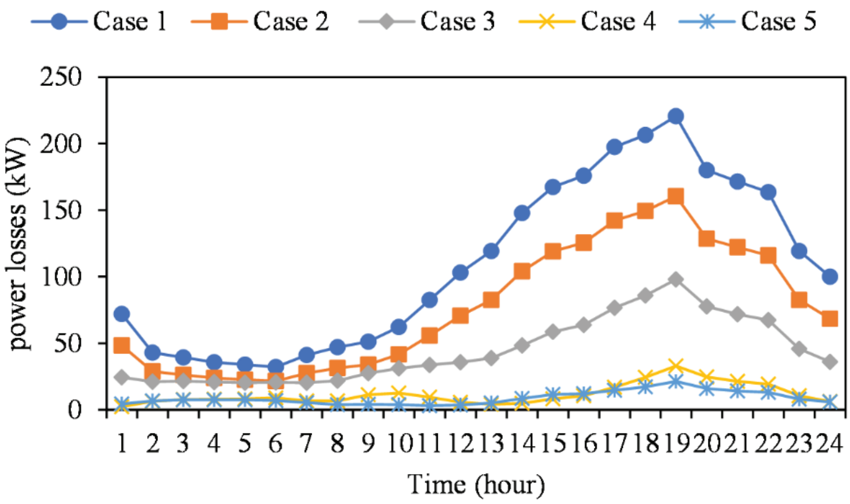

Figure 7. Active power losses across different cases for 69 bus system.

losses during peak demand (18-21), and Case 5 keeping the lowest losses throughout the 24-hour period. This clearly shows that the integrated approach combining RES, CBs, and DNR works better to reduce system losses in both network configurations.

Figures 8 and 9 show a full voltage profile analysis of the IEEE 33-bus and IEEE 69-bus distribution systems at low loading conditions (6:00). They show that different optimization cases have different performance patterns. For the IEEE 33 bus system, Case 1 (the base case) has the worst voltage profile, with values reducing to about 0.97 p.u. With capacitor banks installation, there is a little improvement, keeping voltages above 0.975 p.u as seen in Case 2. Case 4 (combined RES and CBs) displays voltages always above 0.99 p.u. Integration of RES, CBs, and DNR shows the best solution, where all volatge maintain above 1.01 pu.

Similarly, IEEE 69 bus system, the integrated approach of Case 5 perform well to improve the voltage profile by combined operation of RES, CBs, and DNR on both distribution networks.

Figures 10 and 11 show a full voltage profile analysis of the IEEE 33-bus and IEEE 69-bus distribution systems during peak loading conditions (19:00). They show that voltage regulation changes a lot depending on the optimization scenario. The IEEE 33 bus system performs the worst in Case 1 (the base case), with voltage levels dropping to about 0.92 p.u. Case 2 (with capacitor banks) yields a little improvement with voltages just above 0.94 p.u. Whereas Case 3 (RES integration) and Case 4 (combined RES and CBs) both achieve better voltage regulation, with minimum voltages of 0.95 p.u. and 0.96 p.u., respectively. Further, integration of NR operation, minimum voltage is raised to

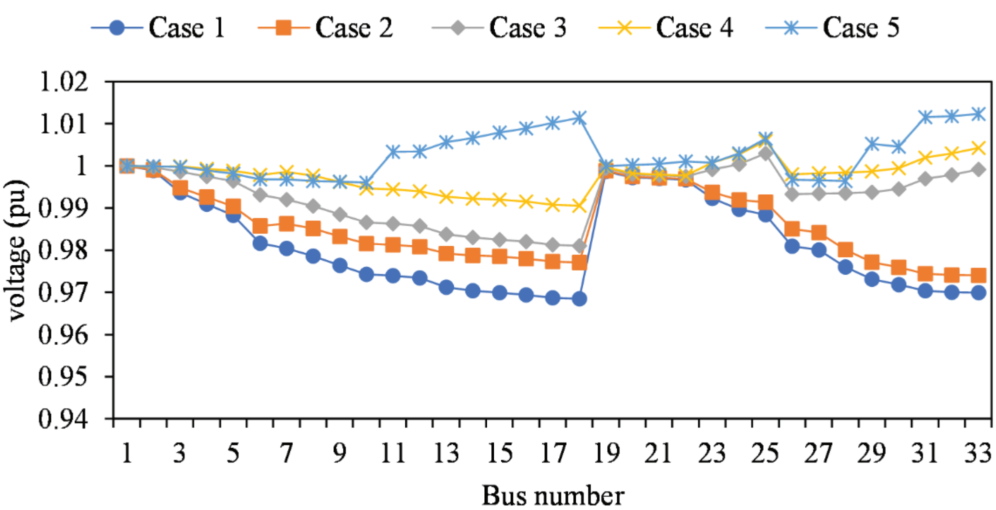

Figure 8. Voltage patterns at different buses at hour 6:00 for 33 bus system.

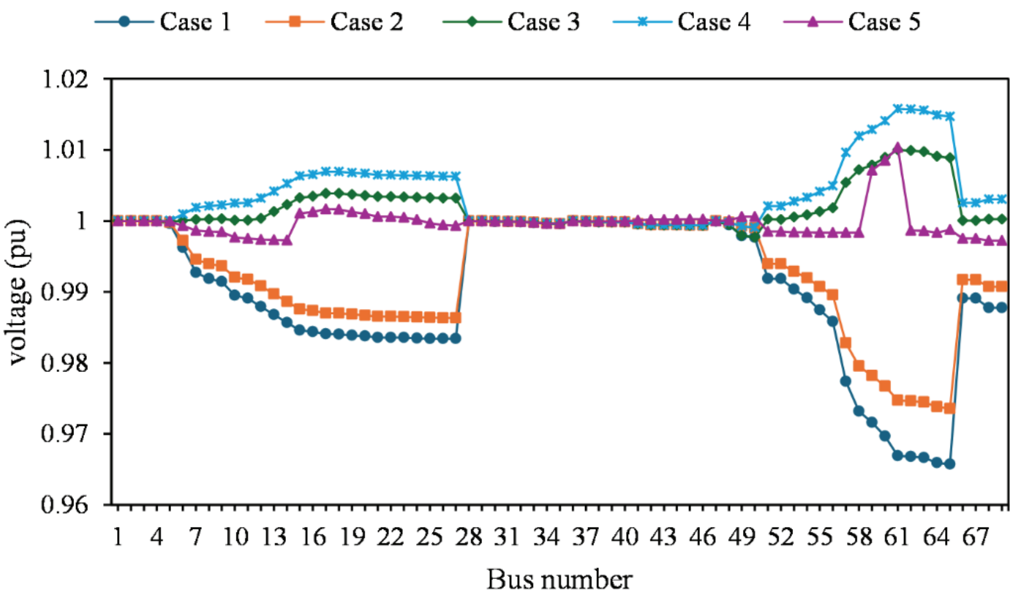

Figure 9. Voltage patterns at different buses at hour 6:00 for 69 bus system.

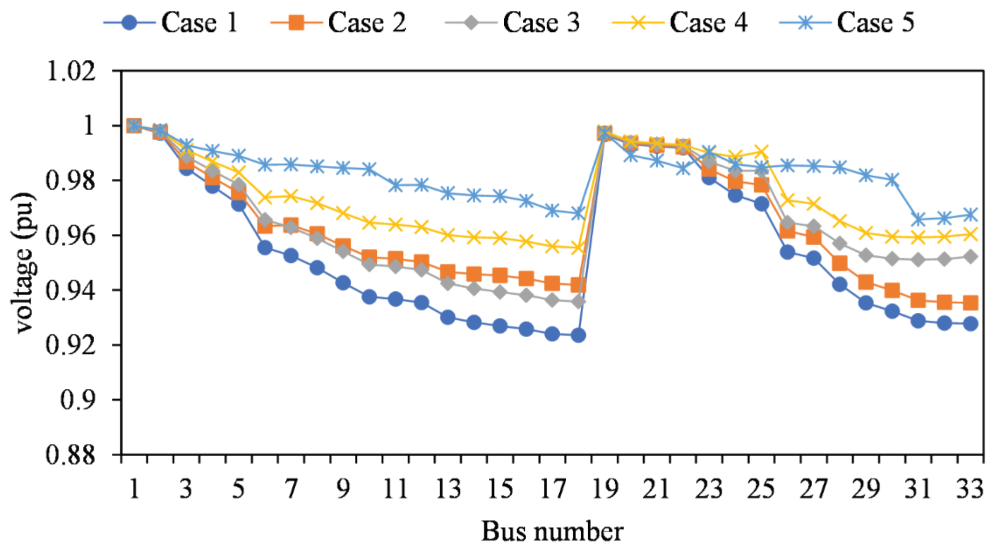

Figure 10. Voltage patterns at different buses at hour 19:00 for 33 bus system.

0.97 pu as seen in Case 5. Similarly, for IEEE 69 bus system, Case 5 yields the most efficient improvement of the voltage profile via the co-ordinated operation of RES, CBs, and DNR, especially under high loading conditions.

Sensitivity Analysis for Uncertainty of Load And PV and Wind Generation

A sensitivity analysis has been conducted to assess system performance among uncertainty. The study analyzed five different cases with 50 unique scenarios, which involved load demand variations and also renewable power generation (PV and wind generation) variation of about ±10% and ±15% respectively. Table 8 displays that the active power losses decreased in all cases. In Case 5, power losses is noted as 391.799 kW, with a standard deviation of 106.354, which is much inferior to the steady 355.394 as observed in Cases 1–4. The minimum voltage magnitude raised from 0.9100 p.u. in Case 1 to 0.9603 p.u. in Case 5, and the standard deviation went down from 0.0031 to 0.0012 as seen in Table 9. Figures 12 and 13 illustration variations of active power losses and minimum voltage of the system under different cases. It is observed, among all

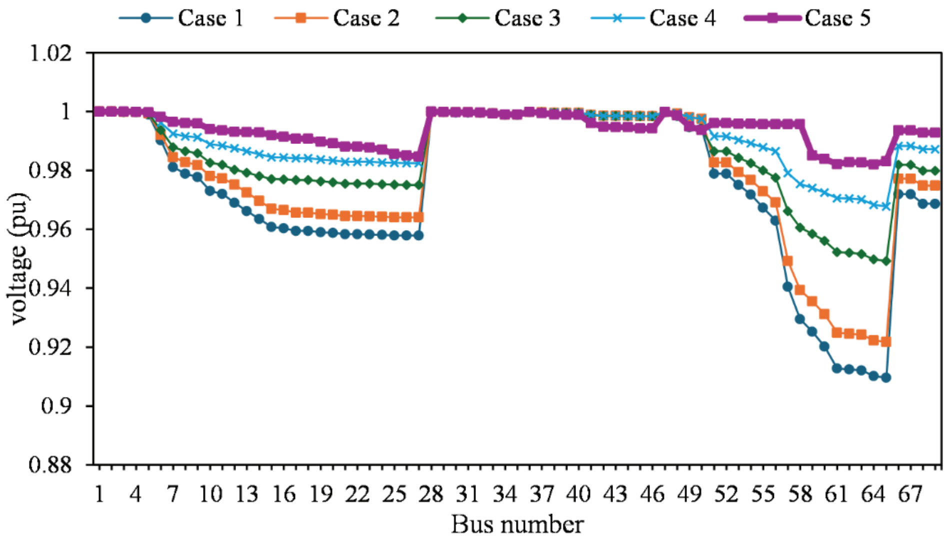

Figure 11. Voltage patterns at different buses at hour 19:00 for 69 bus system.

Table 8. Sensitivity analysis impact on active power losses for 33 bus system

Cases	Case 1	Case 2	Case 3	Case 4	Case 5
Minimum power losses (kW)	2050.599	1713.754	1130.875	748.271	391.799
Standard deviation on power losses (kW)	355.394	355.394	355.394	355.394	106.354

Table 9. Sensitivity analysis impact on minimum voltage magnitude for 33 bus system

Cases	Case 1	Case 2	Case 3	Case 4	Case 5
Minimum voltage (pu)	0.9100	0.9330	0.9390	0.9438	0.9603
Standard deviation on Minimum voltage (pu)	0.0031	0.0031	0.0031	0.0031	0.0012

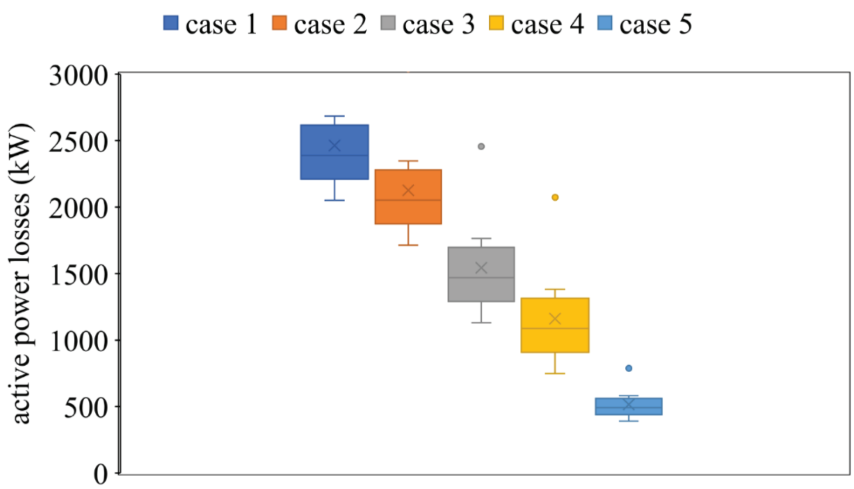

Figure 12. Sensitivity analysis of active power losses of the system under cases for 33 bus system.

Figure 13. Sensitivity analysis of minimum voltage of the system under cases for 33 bus system.

cases, case 5 performed has a very stable performance with less variations.

Evaluation of Proposed Multi COA and Other Metaheuristic Approaches

Due to the complexity of case 5, we evaluated the efficacy of various metaheuristic algorithms, including GA [6], MPA [12], ACA [14], HBA [15], WHO [16], and multi-COA. Table 10 shows the minimum, average, and standard deviation values for these algorithms. Also, Figure 14 shows how each algorithm converges. The suggested multi-COA always gets close to its lowest value, which is $2478.800. In comparison, GA [6], MPA [12], ACA [14], HBA [15], and WHO [16], converge at $3237.290, $3062.112, $2791.250, $2807.370, and $2660.637, respectively.

To evaluate the computational efficiency of different metaheuristic methods, from [34] effective convergence runtime metric has been employed, which provides a standardized measure of convergence speed. This metric is mathematically expressed as given in equation (42)

$$T_{con} = \frac{iter_{con}}{iter_{max}} T_{av} \tag{42}$$

where *Tcon* represents the convergence time, Tav denotes the average time across multiple runs, itercon indicates the number of iterations until convergence, and itermax represents the maximum number of iterations allowed.

A glance at the convergence times shows that the suggested multi-COA method works better. The algorithm

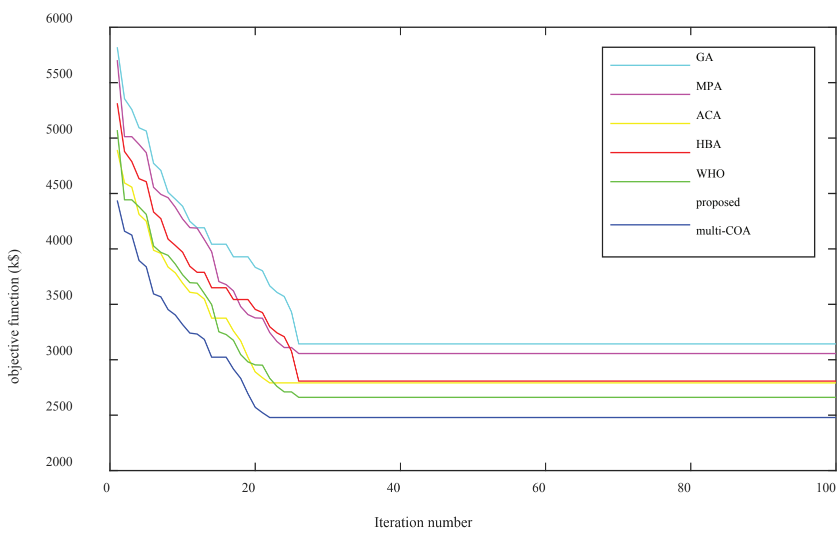

Figure 14. Convergence patterns for each algorithm for 33 bus system.

Table 10. Comparative analysis of several metaheuristic methodologies for 33 bus system

Metaheuristic approach	Minimum value ($\times 10^3$ \$)	Mean value ($\times 10^3$ \$)	Standard deviation ($\times 10^3$ \$)	$Iter_{con}$	T_{con} (minutes)	T_{av} (minutes)
GA [6]	3237.29	3435.956	591.865	30	4.505	15.017
MPA [12]	3062.112	3306.072	556.07	28	4.097	14.633
ACA [14]	2791.25	2984.358	453.087	27	3.884	14.387
HBA [15]	2807.37	3081.745	554.324	23	3.211	13.960
WHO [16]	2660.637	2888.436	506.543	25	3.713	14.853
Proposed multi-COA	2478.8	2658.761	422.243	21	2.795	13.310

always converges in 13.31 minutes, which means it is faster than other well-known metaheuristic methods. Table 8 shows that other methods take longer to converge. For example, GA takes 15.017 minutes, MPA takes 14.633 minutes, ACA takes 14.387 minutes, HBA takes 13.960 minutes, and WHO takes 14.853 minutes. These results show that the proposed multi-COA method is better at converging when dealing with complex optimization problems. This shows that the suggested multi-COA works better than other published metaheuristic methods.

The effectiveness of the multi-COA can be attributed to its ability to balance diversification and intensification while keeping track of previous bests, enabling it to produce results significantly closer to the global optimum.

Performance Comparison of the Proposed Multi-Coa Method with Published Optimization Techniques

Table 11 presents the results, demonstrating that the proposed multi-COA method outperforms other published approaches in the literature. The optimizer finds the best places for three DGs at buses 8, 25, and 32, with sizes of 1.1413 MW, 1.1192 MW, and 0.7517 MW, respectively, by moving the tie switches to positions 4, 13, 11, 15, and 26. The optimal locations for capacitors are also found at buses 8, 25, and 30, with capacities of 0.5437 MVAR, 0.4456 MVAR, and 0.9497 MVAR, respectively. At critical bus 13, minimum bus voltage magnitude is improved to 0.9916 p.u., and the active power loss is dropped to 7.9268 kW. The suggested method attains a loss reduction of up to 96.09% compared to the base case. This is better than other existing

Table 11. Comparative analysis of proposed Multi-COA method with published optimization techniques for 33 bus system

Methods	Base case	GA [6]	SHADE [17]	BPSO [20]	DE [21]	Proposed multi-COA method
Power loss (kW)	202.6	50.149	12.7	15.47	15.63	7.9268
% loss reduction	-----	75.24	93.73	92.36	92.29	96.09
DGs Size (MW) (Position)	-------	0.25 (16), 0.25 (22), 0.5 (30),	1.532 (29), 0.721 (8), 0.641 (16)	0.70 (15), 0.60 (31), 0.70 (25)	0.557 (15), 0.813 (25), 0.630 (32)	1.1413 (8), 1.1192 (25), 0.7517 (32)
SCs Size (MVAR) (Position)	-------	0.3 (15), 0.3 (18), 0.3 (29), 0.6 (30), 0.3 (31)	1.260 (30), 0.236 (14), 0.197 (2)	0.382 (14), 1.013 (30), 0.419 (24)	0.703 (3), 0.399 (9), 0.1198 (30)	0.5437 (8), 0.4456 (25), 0.9497 (30)
Switches opened	33,34,35,36,37	7, 9, 15, 27, 34	11,25,33, 34,35	7,35,10, 36,26	7, 11, 12, 17, 26	4, 13, 11, 15, 26
Min. Bus Voltage (p.u.)	0.9131(18)	0.981	0.9936	0.9887	0.9863 (8)	0.9916(13)

Table 12. Comparative analysis of long-term emission costs (×10^3\$) over a ten-year period for different system cases for 33 bus system

Year	Case 1	Case 2	Case 3	Case 4	Case 5
Year 1	889.912	890.356	359.206	356.251	345.663
Year 2	952.2058	952.6809	384.3504	381.1886	369.8594
Year 3	1014.5	1015.006	409.4948	406.1261	394.0558
Year 4	1076.794	1077.331	434.6393	431.0637	418.2522
Year 5	1139.087	1139.656	459.7837	456.0013	442.4486
Year 6	1537.768	1538.535	620.708	615.6017	597.3057
Year 7	1617.504	1618.311	652.8928	647.5218	628.2771
Year 8	1697.24	1698.087	685.0777	679.4419	659.2485
Year 9	1776.976	1777.863	717.2625	711.362	690.2199
Year 10	2896.471	2897.916	1169.138	1159.52	1125.058

methods such as GA[6], DE [21], BPSO [20], and SHADE [17], which only reduce losses by 75.24%, 92.29%, 92.36%, and 93.73%, respectively.

Long-Term Environmental Impact and Sustainability Analysis

A comprehensive analysis has been conducted to show the environmental impacts and sustainability metrics over 10 years. It is assumed that, there is 7% annual increase in demand. Table 12 depicts the analysis of the emission costs for different cases, where Case 5 performs much better for the environment than the other cases. In year 1, Case 5 achieved 61.2% drop in emission costs at first, which is reduced from $345.663 to $889.912. Further, the cost of emissions had dropped by 61.1%, from $2,896.471 to $1,125.058 by the year 10. Cases 3 and 4, where we incorporated renewable energy sources, were much better for the environment than the base case and capacitor-only scenarios (Cases 1 and 2). Further, with combination of renewable energy sources, capacitor placement, and network reconfiguration to keep the lowest emission costs as seen in Case 5.

CONCLUSION

This study investigated the coordinated planning of renewable energy sources (RES) and capacitor banks within distribution networks by developing a two-level optimization framework for an integrated planning model, while also analysing the impact of network reconfiguration (NR). Simulation results demonstrated the feasibility and efficiency of the proposed model and the multi-layer Crayfish Optimization Algorithm (COA) solver. The coordinated allocation of RES and capacitors led to significant cost reductions of approximately 43% and 59% in IEEE 33 bus and 69 bus distribution systems, respectively, compared to the base case, highlighting the benefits of integrating RES and capacitors rather than deploying them individually. Further, the inclusion of NR operation increased savings to 51% and 61%, respectively. The proposed method was also compared against other existing methods in the literature and performed well, with a significant reduction in power losses. In conclusion, combined operation of NR along with coordinated planning of capacitor banks and RES not only made the distribution systems more reliable, flexible, and environmentally friendly, but it also made them more cost-effective.

Future Scope And Limitations

The suggested framework has a good scope for improvement in the future because it can be easily incorporated with more advanced structures such as market participation, energy storage integration, real-time SCADA optimization and blockchain-based trading methods. Further, technical developments will comprise adding cloud-based optimization, multi-agent architectures, impact of very bad weather, and machine learning for predictive analytics,. There are also market application opportunities, such as offering more services, integrating demand response, peer-to-peer energy trading platforms, and dynamic tariff optimization. All of these would make the framework more useful in energy markets that are changing, while still being able to lower costs and make systems better. Possible limit of present methodology is much computing power is needed to handle data, especially for larger complex distribution systems.

ABBREVIATIONS AND NOMENCLATURE

std	Standard
amb	Ambient
cell	Cell temperature
ci	Cut-in
co	Cut-out
rated	Rated values
P_{pv}	Output power of PV panel [kW]

std	PV power under standard test conditions [kW]
δ	Temperature coefficient of power [%/°C]
Tcell, Tamb, OCT	PV cell temperature [°C] Ambient temperature [°C] Nominal operating cell temperature [°C]
PWG	Output power of wind generator [kW]
a, b	Linear coefficient and Cubic coefficient for wind power curve
vci, vco and vrated	Cut-in wind speed [m/s], Cut-out wind speed [m/s], Rated wind speed [m/s]
PnWG,rated	Rated power of wind generator [kW]
n	Power law exponent
i , *s*	Notation for bus, scenario
s	Notation for scenario
T,t	Notation for Total time duration, time
Dy	Number of days in year
Ω_{bus} *and* Ω_{cap}	Set of buses/ set of buses mounted with capacitor banks
Ω_{Wd} *and* Ω_{PV}	set of buses mounted with wind and PV generation
P_L^{act}, Q_L^{act}	Actual active and reactive power load
V_{act}	Actual voltage
k^p, k^q	Exponents of active and reactive power
μ_p, μ_q *and* σ_p, σ_q	Mean and standard deviation of active power and reactive power
N_{ds}	Total number of decreased scenarios
π_s	Probability of scenario
$Q_{cap,i}^{max}$ $P_{Wd,i}^{max}$ and $P_{PV,i}^{max}$	maximum capacity of capacitor banks, wind based DG and PV based DG respectively at i^{th} bus
$C_{cap}^{inv}, C_{WD}^{inv}, C_{PV}^{inv}$	Investment cost of capacitor bank, Wind and PV based DG
$C_{Cap}^{OM,t}, C_{WD}^{OM,t}, C_{PV}^{OM,t}$	Cost of operation and maintenance of capacitor bank, Wind and PV based DG
$C_{sub}^t, C_{emis}, C_{loss}, C_{ens}$	Cost of substation, emission, losses and energy not served
$Q_{cap,i}^{rated}$, $P_{Wd,i}^{rated}$ and $P_{PV,i}^{rated}$	rated capacity of capacitor banks, wind and PV based DG respectively at i^{th} bus
V^{min}, V^{max}	Minimum and maximum bus voltage magnitude
I_l^{rated}	Rated current in the line *l*
$I_{l,s}^t$,	Current flow in line at time t in scenario
$P_{loss,s}^t, P_{ens,s}^t, P_{sub,s}^t$	Power loss, energy not served, power from substation at t^{th} hour for s^{th} scenario
$Q_{cap,i,s}^t, P_{WD,i,s}^t, P_{PV,i,s}^t$	Reactive power from capacitor bank, active power from wind and PV based DG at t^{th} hour for s^{th} scenario
$P_{i,s}^t, Q_{i,s}^t$	Active/ reactive power at i^{th} bus at t^{th} hour for s^{th} scenario
$V_{i,s}^t$	Voltage magnitude at i^{th} bus at t^{th} hour for s^{th} scenario
G_{ij}, B_{ij}	Real part and imaginary part of admittance matrix element between buses i and j
$P_{i,s}^{D,t}, Q_{i,s}^{D,t}$	Active/ reactive power demand at i^{th} bus at t^{th} hour for s^{th} scenario

AUTHORSHIP CONTRIBUTIONS

Authors equally contributed to this work.

DATA AVAILABILITY STATEMENT

The authors confirm that the data that supports the findings of this study are available within the article. Raw data that support the finding of this study are available from the corresponding author, upon reasonable request.

CONFLICT OF INTEREST

The author declared no potential conflicts of interest with respect to the research, authorship, and/or publication of this article.

ETHICS

There are no ethical issues with the publication of this manuscript.

STATEMENT ON THE USE OF ARTIFICIAL INTELLIGENCE

Artificial intelligence was not used in the preparation of the article.

REFERENCES

[1] Werkie YG, Kefale HA. Optimal allocation of multiple distributed generation units in power distribution networks for voltage profile improvement and power losses minimization. Cogent Eng 2022;9:2091668. [CrossRef]

[2] Iftikhar MZ, Imran K, Akbar MI, Ghafoor S. Optimal distributed generators allocation with various load models under load growth using a meta-heuristic technique. Renewable Energy Focus 2024;49:100550. [CrossRef] [

[3] Pawar A, Viral RK, Bansal M. Capacitor allocation in radial distribution system using modified grey wolf optimization. In: 2024 International Conference on Integrated Circuits and Communication Systems (ICICACS). IEEE; 2024. p. 1–7. [CrossRef]

[4] Pawar A, Viral RK, Mishra A. Distribution expansion planning in a deregulated environment. In: Tomar A, Malik H, Kumar P, Iqbal A, editors. Machine Learning, Advances in Computing, Renewable Energy and Communication. Singapore: Springer; 2022. p. 1–15. [5] Ayanlade SO, Ariyo FK, Jimoh A, Akindeji KT, Adetunji AO, Ogunwole EI, et al. Optimal allocation of photovoltaic distributed generations in radial distribution networks. Sustainability 2023;15:13933. [CrossRef]

[6] Saonerkar AK, Bagde BY. Optimized DG placement in radial distribution system with reconfiguration and capacitor placement using genetic algorithm. In: 2014 IEEE International Conference on Advanced Communications, Control and Computing Technologies. IEEE; 2014. p. 1077–1083. [CrossRef]

[7] Pawar A, Viral RK, Mishra A. Analysis of renewable generation uncertainty for planning and operation. In: Image Processing for the Analysis of Renewable Energy Resources. Sharjah: Bentham Science Publishers; 2022. p. 14–30. [CrossRef]

[8] Yusupov Z, Almagrahi N. Techno–economic and environmental analysis of microgrid: A case study of Karabuk University. Sigma J Eng Nat Sci 2023;41:1-15. [CrossRef]

[9] Abdalı A, Mazlumı K, Noroozıan R. A precise fault location scheme for low-voltage dc microgrids systems using multi-layer perceptron neural network. Sigma J Eng Nat Sci 2018;36:821–834.

[10] Pawar A, Viral RK, Bansal M. Multiple distributed generator allocation for energy loss reduction considering practical load models: A hybrid approach. In: 2024 1st International Conference on Innovative Sustainable Technologies for Energy, Mechatronics, and Smart Systems (ISTEMS). IEEE; 2024. p. 1–6. [CrossRef]

[11] Abbas G, Wu Z, Ali A. Multi-objective multi-period optimal site and size of distributed generation along with network reconfiguration. IET Renewable Power Gener 2024;18:1–15. [CrossRef]

[12] Dharavat N, Sudabattula SK, Suresh V. Optimal integration of distributed generators (DGs) shunt capacitors (SCs) and electric vehicles (EVs) in a distribution system (DS) using marine predator algorithm. Int J Renewable Energy Res 2022;12:1805–1818.

[13] Kamel S, Khasanov M, Jurado F, Kurbanov A, Zawbaa H.M, Alathbah MA. Simultaneously distributed generation allocation and network reconfiguration in distribution network considering different loading levels. IEEE Access 2023;11:1–15. [CrossRef]

[14] Saravanan C, Vengadachalam N, Balakrishnan P, Sathyanarayanan TKS. Enhancing distribution network efficiency with Andean condor algorithm-driven optimal placement of distributed generation and network reconfiguration. Electric Power Components and Systems 2024;2024:1–17. [CrossRef]

[15] Thumati S, Vadivel S, Rao M. Honey badger algorithm based network reconfiguration and integration of renewable distributed generation for electric vehicles load penetration. International Journal of Intelligent Engineering & Systems 2022;15:1–12. [CrossRef]

[16] Ali MF, Beshr E, Abdelaziz AY, Ezzat M. Hybrid siting and sizing of distributed generators and shunt capacitors with system reconfiguration using wild horse optimizer. Journal of Advanced Research in Applied Sciences and Engineering Technology 2024;38:196–213. [CrossRef]

[17] Sayed MM, Mahdy MY, Abdel Aleem SH, Youssef HK, Boghdady TA. Simultaneous distribution network reconfiguration and optimal allocation of renewable-based distributed generators and shunt capacitors under uncertain conditions. Energies 2022;15:2299. [CrossRef]

[18] Ramadan A, Ebeed M, Kamel S, Nasrat L. Optimal allocation of hybrid solar-wind distributed generations in distribution networks considering the uncertainty using grasshopper optimization algorithm. In: 2019 21st International Middle East Power Systems Conference (MEPCON). IEEE; 2019. p. 406–410. [CrossRef]

[19] Fathi R, Tousi B, Galvani S. A new approach for optimal allocation of photovoltaic and wind clean energy resources in distribution networks with reconfiguration considering uncertainty based on info-gap decision theory with risk aversion strategy. J Cleaner Prod 2021;295:125984. [CrossRef]

[20] Essa MB, Alnabi LA, Dhaher AK. Distribution power loss minimization via optimal sizing and placement of shunt capacitor and distributed generator with network reconfiguration. TELKOMNIKA 2021;19:1039–1049. [CrossRef]

[21] Biswas PP, Suganthan PN, Amaratunga GAJ. Distribution network reconfiguration together with distributed generator and shunt capacitor allocation for loss minimization. In: 2018 IEEE Congress on Evolutionary Computation (CEC). IEEE; 2018. p. 1–7. [CrossRef]

[22] Saravanan C, Vengadachalam N, Balakrishnan P, Sathyanarayanan TKS. Enhancing distribution network efficiency with Andean condor algorithm-driven optimal placement of distributed generation and network reconfiguration. Electric Power Components and Systems 2024;2024:1–17. [CrossRef]

[23] Iftikhar MZ, Imran K, Akbar MI, Ghafoor S. Optimal distributed generators allocation with

various load models under load growth using a meta-heuristic technique. Renewable Energy Focus 2024;49:100550. [CrossRef]

[24] Maurya P, Tiwari P, Pratap A. Electric eel foraging optimization algorithm for distribution network reconfiguration with distributed generation for power system performance enhancement considerations different load models. Comput Electr Eng 2024;119:109531. [CrossRef]

[25] Pratap A, Tiwari P, Maurya R, Singh B. Crayfish optimisation algorithm for strategic planning of distributed generation and capacitor bank with network reconfiguration on radial distribution network. International Journal of Ambient Energy 2024;45:2392620. [CrossRef]

[26] Li R, Wang W, Wu X, Tang F, Chen Z. Cooperative planning model of renewable energy sources and energy storage units in active distribution systems: A bi-level model and Pareto analysis. Energy 2019;168:30–42. [CrossRef]

[27] Pamshetti VB, Singh SP. Integrated operation and planning model of renewable energy sources with flexible devices in active distribution networks. In: Flexibility in Electric Power Distribution Networks. Boca Raton: CRC Press; 2021. p. 255–285. [CrossRef]

[28] Pamshetti VB, Singh SP. Coordinated allocation of BESS and SOP in high PV penetrated distribution network incorporating DR and CVR schemes. IEEE Systems Journal 2022;16:420–430. [CrossRef]

[29] Jia H, Rao H, Wen C, Mirjalili S. Crayfish optimization algorithm. Artif Intell Rev 2023;56:1919–1979. [CrossRef]

[30] Baran ME, Wu FF. Network reconfiguration in distribution systems for loss reduction and load balancing. IEEE Transactions on Power Delivery 1989;4:1401–1407. [CrossRef]

[31] Sivanagaraju S, Visali N, Sankar V, Ramana T. Enhancing voltage stability of radial distribution systems by network reconfiguration. Electr Power Compon Syst 2005;33:539–550. [CrossRef]

[32] Padilha-Feltrin A, Rodezno DAQ, Mantovani JRS. Volt-VAR multiobjective optimization to peak-load relief and energy efficiency in distribution networks. IEEE Transactions on Power Delivery 2014;30:618–626. [CrossRef]

[33] National Renewable Energy Laboratory. Renewable energy sources data. Washington: NREL; 2026.

[34] Esmaeilian HR, Fadaeinedjad R. Energy loss minimization in distribution systems utilizing an enhanced reconfiguration method integrating distributed generation. IEEE Systems Journal 2014;9:1430–1439. [CrossRef]